Water Air Soil Pollut (2020) 231: 72
https://doi.org/10.1007/s11270-020-4402-8

Decolorization of the Reactive Blue 19 from Aqueous Solutions with the Fenton Oxidation Process and Modeling with Deep Neural Networks

Nejdet Değermenci · **Kemal Akyol**

Received: 2 October 2019 / Accepted: 6 January 2020 / Published online: 3 February 2020

Abstract The decolorization of Reactive Blue 19 (RB19) from aqueous solutions using the Fenton oxidation process was researched. The effects of different operating parameters, e.g., H_2O_2, Fe(II), initial dye concentration, pH, and solution temperature, on the decolorization of RB19 were investigated. Increasing, the H_2O_2 concentration and temperature increased the rate of the decolorization; however, increasing initial RB19 concentration reduced the decolorization. Additionally, modeling of the decolorization obtained by the Fenton oxidation process was researched based on deep neural networks (DNN) architecture providing the best performance in terms of optimum hidden layers and neuron numbers in addition to ideal activation and optimization function pairs. The performances of the models were analyzed on the training, validation, and test data. According to the experimental results, the seven hidden layers DNN model with "relu" activation function and "RMSProp" optimization function provided the best performance with root mean square error (RMSE) of 3.39 and correlation coefficient (R^2) of 0.99.

Keywords Wastewater treatment · Decolorization · Reactive blue 19 · Deep neural networks

N. Değermenci (✉)
Department of Environmental Engineering, Kastamonu University, Kastamonu, Turkey
e-mail: ndegermenci@gmail.com

K. Akyol
Department of Computer Engineering, Kastamonu University, Kastamonu, Turkey

1 Introduction

A variety of synthetic dyes with different chemical characteristics are used in textile, plastic, cosmetic, pharmaceutical, leather, and food industries (Baştürk and Alver 2019; Siddique et al. 2014). Dyes with many structural varieties are important pollutant sources causing environmental pollution. Reactive dyes represent nearly 30% of synthetic dyes worldwide. They contain a functional group comprising molecular structures, a chromophore group, and covalent bonds with cellulose fibers (Değermenci et al. 2019). RB19, easily obtained and commonly used in the textile industry, is an anthraquinone-based dye and is more resistant to biological degradation due to fused aromatic structures compared to azo-based dyes (Xie et al. 2019; Fanchiang and Tseng 2009). During dye processes, nearly 15% of dye loss occurs and this dye mixes with wastewater (Bhatti et al. 2013). Wastewater containing synthetic dyes comprises a danger to ecosystems due to surface active matters, solvents, mineral salts, and acids they contain. Some dyes cause allergic dermatitis, skin irritation, mutations, and cancer in humans. When wastewater containing synthetic dyes are discharged into the receiving environment without the use of appropriate treatment methods, photosynthesis of plants living in water is prevented due to the reduction in light transmission, causing anoxic conditions deadly for aquatic organisms due to depletion of dissolved oxygen, the esthetic appearance of the water is disrupted, and possibilities to reuse water are limited (Wang et al. 2007; Suteu et al. 2012; Hayat et al. 2015; Nidheesh et al.

2018). As a result, treatment of wastewater containing dyes before discharging into the receiving environment is of great importance.

For removal of dye from wastewater, a variety of physical, chemical, and biological methods or combinations of them have been developed like chemical precipitation, electrocoagulation, membrane filtration, adsorption, ozonation, and aerobic and/or anaerobic treatment (Hu et al. 2006). Physicochemical methods for treatment of these wastewaters are accepted as more expensive than biological treatment methods; however, biological treatment methods are insufficient for removal of color-giving substances and other stubborn compounds (Bae et al. 2015). Chemical degradation with oxidative agents like chlorine is one of the most important and effective methods; however, it produces many toxic products like organochlorine compounds (Slokar and Le Marechal 1998). Industrial application of ozonation is limited by high production and operating costs and weak mass transfer (Zhang et al. 2006). Advanced oxidation processes (AOP) have high potential for removal of organic pollutants from aqueous solutions. In recent times, AOP for wastewater treatment has been intensely researched because AOPs may oxidize compounds that are difficult to degrade. The Fenton oxidation process is one of these AOPs and is used for treatment of different industrial wastewaters (pharmaceutical, textile, chemical, paper pulp, food processing, landfill leachate, etc.) (Ghosh et al. 2010; Vilar et al. 2013). The Fenton oxidation process is accepted as one of the simple and appropriate-cost AOPs for industrial wastewater treatment (Azbar et al. 2004; Şahinkaya 2013; Sanchis et al. 2014). The Fenton oxidation process can occur at environmental temperatures and does not require energy input, and reagents are easily obtained (Vilar et al. 2013).

The Fenton oxidation process occurs in four stages including setting pH, oxidation, neutralization, and coagulation (Özdemir et al. 2010). The oxidation mechanism is based on production of hydroxyl radicals as a result of the reaction of H_2O_2 with a Fe(II) catalyst under acidic conditions "Eq. 1" (Bayhan and Degermenci 2017). Hydroxyl radicals are very reactive and unselective oxidants that can oxidize organic matter (Chavaco et al. 2017). Hydroxyl radicals attack unsaturated dye molecules, destroy chromophore and chromogens in dye molecules, and remove color (Emami et al. 2010). The basic advantage of the Fenton oxidation process is the ability to definitively transform pollutants into harmless compounds (CO_2, H_2O, inorganic salts, etc.) (Ghosh et al. 2010):

$$Fe^{2+} + H_2O_2 + H^+ \rightarrow Fe^{3+} + OH^{\bullet} + H_2O \quad (1)$$

An artificial neural network (ANN) is a method used to define the relationship between operating parameters and process performance (Radwan et al. 2018). So far in many studies, the ANN-based models have been designed in order to examine the water and wastewater treatment processes. For example, Alver and Kazan (2020) examined the efficiency of a full-scale filtration plant by using some water quality parameters. They eliminated the organic compounds and anions by Ultrafiltration and Reverse Osmosis processes. Also, they sent the influent water quality parameters obtained by principal component analysis to the artificial neural networks model in order to evaluate the treatment plant efficiency. Daneshvar et al. (2006) successfully predicted the decolorization from aqueous solutions containing Basic Yellow 28 with the electrocoagulation process using an ANN model. Another study by Elmolla et al. (2010) predicted the antibiotic degradation in terms of chemical oxygen demand removal by the Fenton oxidation process. Finally, Mousavi et al. (2018) determined the optimum operating conditions for Methylene Blue removal with the Fenton process using ANN. Deep learning based on the theoretical basis of ANN architecture is a very superior algorithm to obtain successful results by extrapolation from data (Ravì et al. 2016). While there is a hidden layer in the ANN architecture, there are multiple hidden layers in the Deep neural networks (DNN) architecture. Since deep learning was first revealed, different deep learning algorithms and approaches have been continuously and rapidly developed. It is stated to be popular for a long time in computer science and many other disciplines. DNN architecture, which is one deep learning algorithm, comprises an input layer, the hidden layers, and an output layer. While there are one or two hidden layer(s) in the ANN architecture, there are multiple hidden layers in the DNN architecture. Typical DNN architecture is given in Fig. 1.

For the decolorization of RB19 with Fenton oxidation, it is necessary to determine the optimum levels for experimental conditions. In this study, the H_2O_2 concentration, Fe(II) concentration, initial RB19 concentration, initial pH, and temperature parameters were

researched for the decolorization with Fenton oxidation to determine the optimum decolorization conditions. Also, DNN-based modeling was performed to estimate experimental results with the aim of contributing to the literature.

2 Materials and Methods

2.1 Chemicals

RB19 was obtained from a textile factory located in Bursa (Turkey) and used without any purification process. The molecular structure and characteristics of RB19 are given in Table 1. Hydrogen peroxide (30%, w/w), iron (II) sulfate heptahydrate, sulfuric acid, and sodium hydroxide were obtained from Sigma-Aldrich. All solutions were prepared using deionized water.

2.2 Experimental Procedure

One of the parameters affecting the decolorization of RB19 with the Fenton oxidation process was changed while the others remained fixed. The reactor used in the experiments was double-walled and operated in batch mode. For each experimental study, Fe(II) and RB19 were diluted to 500 mL with deionized water and then set to the desired pH using 0.5 M H_2SO_4 and NaOH with a pH meter (WTW, MultiLine Multi 3620 IDS). Then, H_2O_2 was added to the reactor to begin the reaction. Samples were periodically removed from the reactor with a pipette and immediately analyzed. With the aim of ensuring homogeneity of the solution in the Fenton oxidation, a magnetic stirrer was used (IKA, RCT basic) to mix at 500 rpm. Temperature was held at the desired value using a fixed temperature-controlled heating-cooling circulator (LABO, C200-H13). Samples taken at 1, 2, 3, 5, 10, 15, 20, 25, 30, 35, 40, 50, 60, 70, 80, 90, 100, 110, and 120 min were used to determine RB19 concentration. Considering the effects of other parameters (initial pH, Fe(II) concentration, H_2O_2 concentration, initial dye concentration, and temperature) with this reaction duration, a dataset was formed by combining 380 samples.

2.3 Analytical Method

RB19 concentrations were determined by measuring absorbance values with a prepared calibration curve at maximum wavelength using a UV-vis spectrophotometer (Hach Lange, DR6000). As the oxidation reaction continued during the Fenton oxidation process, absorbance measurements were completed immediately after obtaining the sample. The decolorization of RB19 was calculated using the following equation (Eq. 2):

$$\text{Decolorization}, (\%) = (1-C_t/C_0) \times 100 \quad (2)$$

Here, C_0 represents initial RB19 concentration, while C_t is the RB19 concentration at time t.

2.4 Model Construction

In this section, ideal activation and optimization functions, and also optimum, the number of hidden layers and neurons were researched. This issue is the most important step in design of the best DNN model. We noted that the number of hidden layers must be at least three for DNN as described in [27]. Otherwise, it would show shallow neural network properties. Within the frame of this context, the performances of DNN models with the 3, 5, and 7 hidden layers were explored one by one with 1000 iterations. Also, the effects of each pair of "tanh," "relu," "sigmoid," and "softsign" activation functions and "RMSprop," "Adagrad," "Adadelta," "Adam," and "Adamax" optimization functions were examined on the model topology. Hence, numerous tests were conducted using the topologies listed in Table 2 on the dataset with "n" input parameters ($n = 6$). We must also state that the DNN model name consists of two words and one digit for easy understanding by readers and researchers. The first one of the words indicates the activation function name, and the second one indicates the name of optimization function. The digit indicates the number of hidden layers. For example, DNN_tanh_Adam_3 model indicates that the tanh activation function, the Adam optimization function, and the "3" hidden layer number. The models were designed by using "Keras" library with "Tensorflow" backend. Keras contains large collections of deep learning architectures. An overview of the flowchart for the proposed approach is given in Fig. 2.

Performances of DNN models were evaluated by utilizing the root means square error (RMSE) and coefficient of determination (R^2) criteria which are given in Eqs. 3 and 4, respectively:

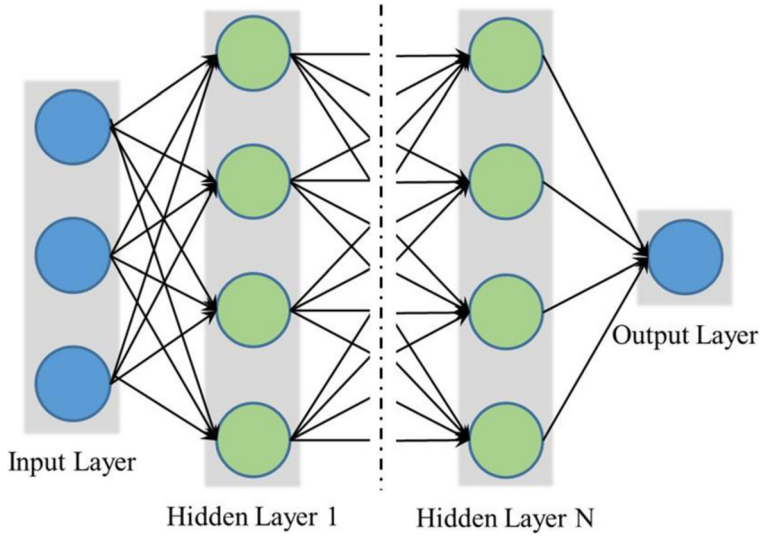

Fig. 1 An overview of the DNN architecture (Ravì et al. 2016)

$$\mathrm{RMSE} = \left[\frac{1}{p}\sum_{i=1}^{p}|e_i|^2\right]^{1/2} \quad (3)$$

Here, p is the number of data points. For RMSE measurement, e_i ($i = 1, 2, \ldots, p$) statistical summaries are taken as reference. Generally, $e_i = P_i - M_i$ defined the estimation error of any model. P_i and M_i are estimated and observed values, respectively (Willmott and Matsuura 2005):

$$R^2 = 1 - \frac{\sum_{i=1}^{p}(\hat{y}-y)^2}{\sum_{i=1}^{p}\left(y-\bar{y}\right)^2} \quad (4)$$

Here, y is the observed result variable, $\bar{y}$ is the mean of this result variable, and $\hat{y}$ is the estimated value for this variable. The coefficient of determination (R^2), frequently used in statistics, is a metric used to measure the fit of a model. This coefficient generally has a value between 0 and 1. A value of 1 shows the model has the perfect fit. This metric measures the degree of variation of the target variable (Alexander et al. 2015).

Table 1 Some characteristics of RB19 (Bhatti et al. 2013)

Properties	Dye
Molecular formula	$C_{22}H_{16}N_2Na_2O_{11}S_3$
Molecular weight	626.533 g/mol
Wavelength	594 nm
Synonym	Remazol Brilliant Blue R
Functional group	Anthraquinone
Molecular structure	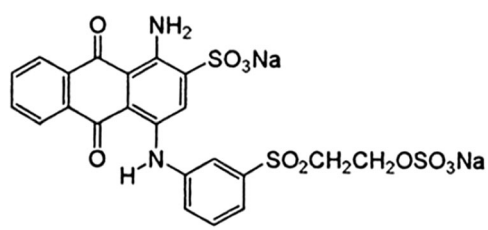

Table 2 An overview of topologies used for DNN models

Hidden layer number	Hidden layer topology
3	$n \rightarrow n^2 \rightarrow n$
5	$n \rightarrow n^2 \rightarrow n^3 \rightarrow n^2 \rightarrow n$
7	$n \rightarrow n^2 \rightarrow n^3 \rightarrow n^4 \rightarrow n^3 \rightarrow n^2 \rightarrow n$

3 Results and Discussion

3.1 Validation and Test of the Model

The input parameters are "time," "H_2O_2," "Fe(II)," "pH," "Dye," and "Temperature" and the target parameter is "Decolorization." The min-max normalization technique given in Eq. 5 was applied to all input data and target data. Thus, the dataset was normalized between 0 and 1:

$$x_n = \frac{x_i - x_{\min}}{x_{\max} - x_{\min}} \tag{5}$$

Here, x_n is the normalized value of x_i and x_{max} and x_{min} indicate the maximum and minimum values of the corresponding parameter.

The dataset which consisted of 380 experimental data points was randomly split into train, validation, and test data by 60%, 20%, and 20%, respectively. Firstly, the DNN models fitted on the validation dataset. Then, the performances of these models were measured on the test dataset. Modeling results obtained by applying different activation functions in hidden layers of DNN and applying different optimization functions for training of DNN are presented in Table 3. The results are also illustrated in Fig. 3.

According to the results, the RMSE values of the models designed with tanh, sigmoid, and softsign activation functions were very high. The relu activation function has shown the best performance. Apart from the "adagrad" optimization function, the increase in hidden layer and neuron numbers in the topologies designed with all optimization functions and relu activation function positively improved the performance of the model. For example, when the layer number is increased from 3 to 5 for the relu activation function and RMSProp optimization function, the neuron number automatically increases and the RMSE decreases from 17.22 to 8.89 while R^2 increases from 0.68 to 0.92. The success obtained from the models with seven

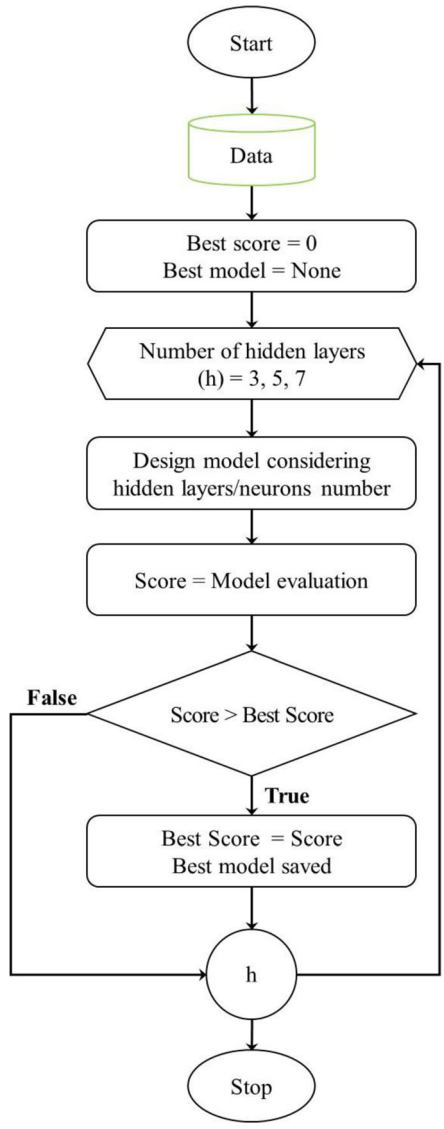

Fig. 2 Flowchart of the proposed study

hidden layers, relu activation function and the Adadelta and RMSProp optimization functions are very close to each other. Therefore, the two models (DNN_relu_Adadelta_7 and DNN_relu_RMSProp_7) with optimal performance could also be applied to estimate the decolorization of RB19.

Also, Fig. 4 depicts the scatter plots of predicted versus actual values of the best models for each activation function on the test dataset. As shown in this figure, DNN_relu_RMSprop_7 fits the actual values excellently. On the other hand, it is seen that both sigmoid and softsign activation functions were unsuccessful. These

figures contain two lines, one is the perfect fit Y = T (predicted data = experimental data) and the other one is the best fit indicated by solid line obtained from the best linear equation Y = (1.07)x − 2.31.

Consequently, the DNN_relu_RMSprop_7 having n-n^2-n^3-n^4-n^3-n^2-n hidden neurons, respectively, was selected as the best DNN model by considering the minimum value of RMSE and the maximum value of R^2 for the testing set. The model with the RMSE and R^2 metrics for actual and predicted values are 3.39 and 0.99 respectively is demonstrated in Fig. 5. It provides acceptable modeling accuracy results for the decolorization prediction. Therefore, this model was saved to the system.

3.2 Effect of Initial pH

The value of pH is an important operating parameter for wastewater treatment and is one of the parameters affecting the hydroxyl radical production rate, H_2O_2, and Fe(II) concentration in the Fenton oxidation process (Behnajady et al. 2007). With the aim of determining the optimum pH value for the decolorization of RB19 with Fenton oxidation, the results obtained from experiments performed with different initial pH values are shown in Fig. 6. The results show the initial pH value of the solution significantly affected the decolorization of RB19. The highest decolorization was obtained with pH 3 as 93.1% at the end of 120 min. Several studies have revealed that the Fenton oxidation process has higher oxidation ability in situations where the solution pH is acidic (Lucas and Peres 2006; Bayhan and Degermenci 2017). However, at values pH < 3, the reactivity of H_2O_2 with Fe(II) may reduce due to the reaction in Eq. 6 and the decolorization of RB19 may slow (Radwan et al. 2018). Additionally, due to the reaction in Eq. 7, the H^+ ions in solution may cause scavenging of hydroxyl radicals which reduces the oxidation efficiency (Michael et al. 2010). Another possibility is that the formation of iron complexes may cause slower reactions with H_2O_2 (Khan et al. 2018). As a result, this may explain the low decolorization of RB19 in the first 30 min at pH 2. However, as for pH > 4, the decolorization may reduce depending on the separation of H_2O_2 into water and oxygen (Eq. 8) and formation of $Fe(OH)_3$ complexes (Eq. 9) (Sun et al. 2007, 2009). Considering the decolorization of RB19, the optimum initial pH value was chosen as 3:

$$H_2O_2 + H^+ \rightarrow H_3O_2^+ \quad (6)$$

$$^{\bullet}OH + H^+ + e^- \rightarrow H_2O \quad (7)$$

$$2H_2O_2 \rightarrow 2H_2O + O_2 \quad (8)$$

$$Fe^{3+} + 3OH^- \rightarrow Fe(OH)_3 \quad (9)$$

Table 3 Experimental results of the different DNN models

		Optimization functions									
		RMSprop		Adagrad		Adadelta		Adam		Adamax	
Activation function	Hidden layer number	RMSE	R^2	RMSE	R^2	RMSE	R^2	RMSE	R^2	RMSE	R^2
tanh	3	30.69	0	48.89	− 1.54	6.53	0.95	19.03	0.62	19.93	0.58
	5	30.68	0	49.03	− 1.55	19.95	0.58	19.58	0.59	19.85	0.58
	7	30.68	0	49.09	− 1.56	30.69	0	30.69	0	30.69	0
relu	3	17.22	0.68	21.34	0.52	15.77	0.74	19.35	0.60	17.07	0.69
	5	8.89	0.92	19.31	0.6	5.97	0.96	14.37	0.78	14.98	0.76
	7	3.39	0.99	63.01	− 3.22	4.82	0.98	9.34	0.91	10.33	0.89
softsign	3	30.68	0	48.60	− 1.51	19.06	0.61	22.28	0.47	30.67	0
	5	30.69	0	48.87	− 1.54	20.17	0.57	30.56	0.01	30.68	0
	7	30.68	0	48.91	− 1.54	19.79	0.58	20.03	0.57	30.31	0.02
sigmoid	3	30.68	0	49.06	− 1.56	30.68	0	20.01	0.57	20.17	0.57
	5	30.69	0	49.05	− 1.56	30.69	0	30.69	0	30.69	0
	7	30.68	0	49.20	− 1.57	30.68	0	30.69	0	30.69	0

3.3 Effect of Fe(II) Concentration

The Fe(II) concentration is an important parameter for the Fenton oxidation process. As a result, with the aim of determining the optimum Fe(II) concentration for the decolorization of RB19, a range of experiments were completed with different Fe(II) concentrations (5, 7.5, 10, 15, and 20 mg/L). The effect of Fe(II) concentration on the decolorization of RB19 is shown in Fig. 7. The results obtained show the decolorization of RB19 is significantly linked to Fe(II). At the end of 120 min with 10 mg/L Fe(II) concentration, maximum decolorization of RB19 was obtained (93.1%). At higher Fe(II) concentrations, the decolorization of RB19 reduced. Studies have shown that the use of high amounts of Fe(II) causes scavenging of hydroxyl radicals due to the reaction in Eq. 10 and leads to a rapid fall in pollutant removal rate (Kavitha and Palanivelu 2005; Bautista et al. 2007), and it has been also reported that it brings about increase in total dissolved solid matter and turbidity (Babuponnusami and Muthukumar 2014; Alalm et al. 2015). Considering the results in Fig. 7, the optimum Fe(II) concentration was chosen as 10 mg/L for the decolorization of 100 mg/L RB19.

$$^{\bullet}OH + Fe^{2+} \rightarrow Fe^{3+} + OH^{-} \quad (10)$$

3.4 Effect of H_2O_2 Concentration

The H_2O_2 concentration plays a very important role in determining the decolorization of dye. While the use

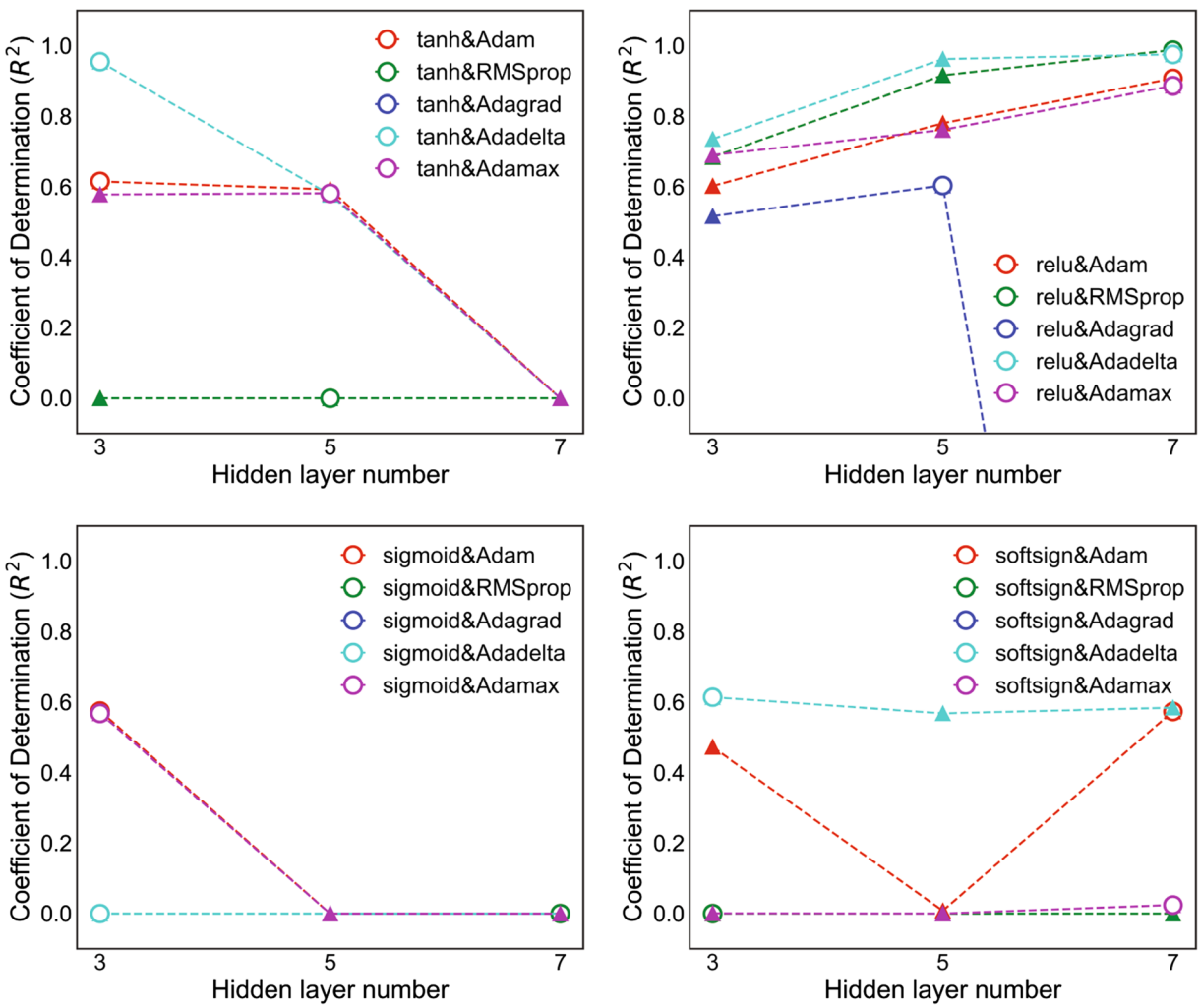

Fig. 3 Results for DNN models having different activation and optimization functions

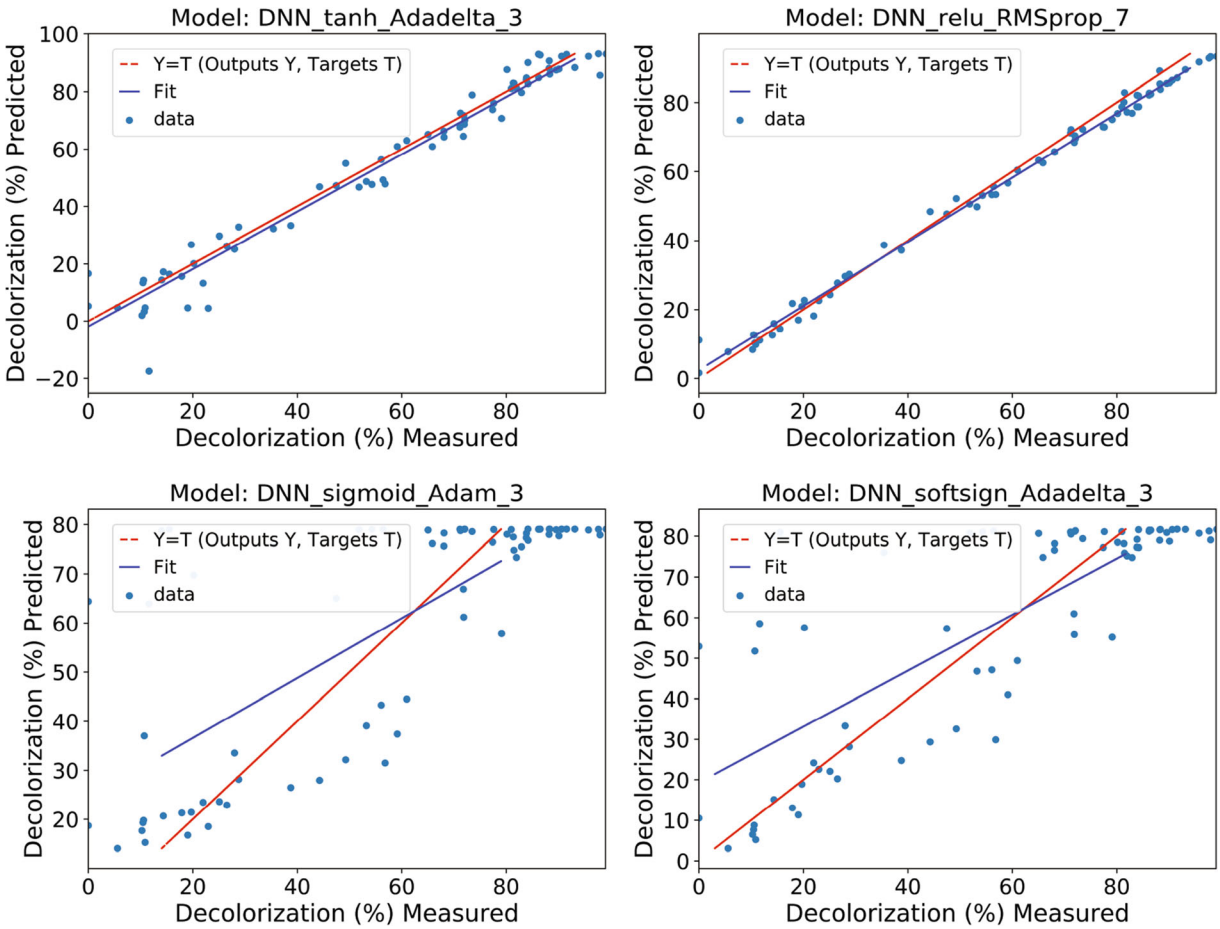

Fig. 4 Scatter plots of predicted versus actual values of the best models for each activation function on the test dataset

of it in low amounts reduces removal efficiency, using it more than necessary augments treatment costs by increasing the residual H_2O_2 concentration (Lin and Lo 1997; Lin and Leu 1999). As a result, it is necessary to determine the optimum H_2O_2 concentration. In line with this aim, a range of experiments were completed with different H_2O_2 concentrations (25, 50, 75, 100, 150, and 200 mg/L) and the results obtained are shown in Fig. 8. The increase in H_2O_2 concentration from 25 to 200 mg/L increased the decolorization of RB19 from 68.5 to 99.5% at the end of 120-min reaction time. This situation can be explained by the increasing H_2O_2 concentration increasing the amount of hydroxyl radicals produced by the Fenton oxidation process (Shi et al. 2018). The use of high amounts of H_2O_2 consumes hydroxyl radicals (Eqs. 11–13) and is

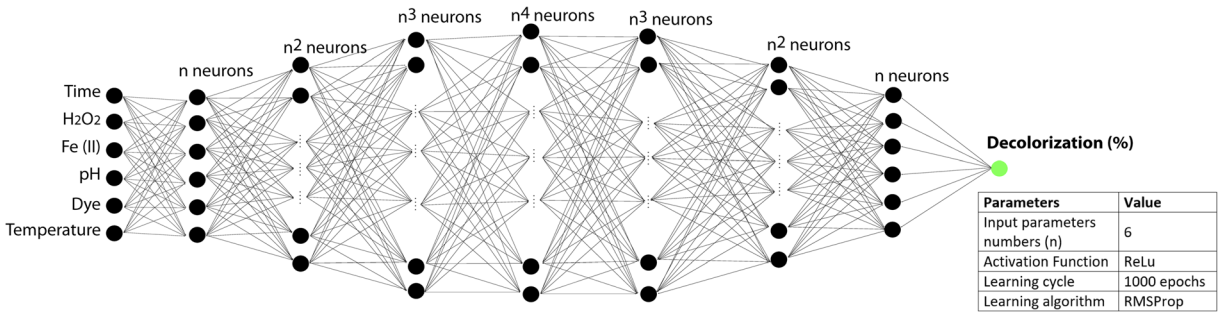

Fig. 5 Optimized DNN architecture

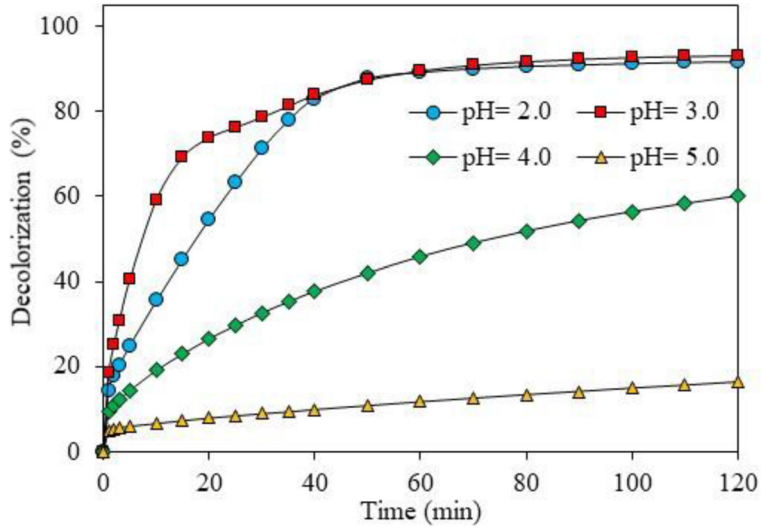

Fig. 6 Effect of initial pH on the decolorization (RB19 = 100 mg/L, H_2O_2 = 100 mg/L, Fe(II) = 10 mg/L, Temperature = 20 °C)

stated to lower removal efficiency (Bautista et al. 2007; Chang and Chern 2010). As a result, considering both consumption of hydroxyl radicals and operating costs, experiments with higher H_2O_2 concentrations were not performed. For 100 mg/L RB19, the optimum H_2O_2 concentration was 100 mg/L with 93.2% decolorization obtained:

$$H_2O_2 + {}^{\bullet}OH \rightarrow {}^{\bullet}HO_2 + H_2O \quad (11)$$

$${}^{\bullet}OH + {}^{\bullet}HO_2 \rightarrow O_2 + H_2O \quad (12)$$

$${}^{\bullet}OH + {}^{\bullet}OH \rightarrow 1/2O_2 + H_2O \quad (13)$$

3.5 Effect of Initial RB19 Concentration

Initial pollutant concentration is an important factor in the Fenton oxidation process. As the concentration of pollutants found in wastewater changes momentarily, it is important to determine the effect of the pollutant concentration entering the treatment process on the treatment efficiency (Titouhi and Belgaied 2016). Figure 9 shows the effect of initial RB19 concentration on the decolorization with the Fenton oxidation process. For 50 mg/L RB19 concentration, 100% decolorization was obtained at the end of 60 min, while the 93.1%, 84.2%, 77.5%, and 72.4% decolorization was obtained at the end of

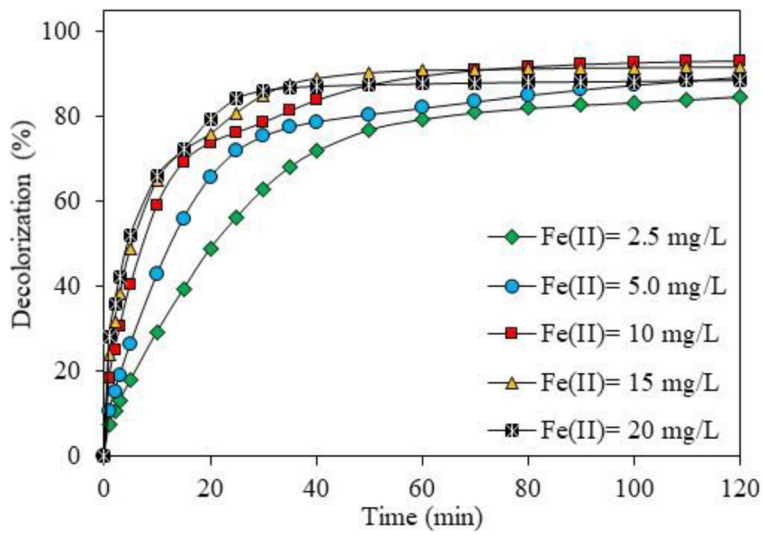

Fig. 7 Effect of Fe(II) on the decolorization (RB19 = 100 mg/L, H_2O_2 = 100 mg/L, pH = 3, Temperature = 20 °C)

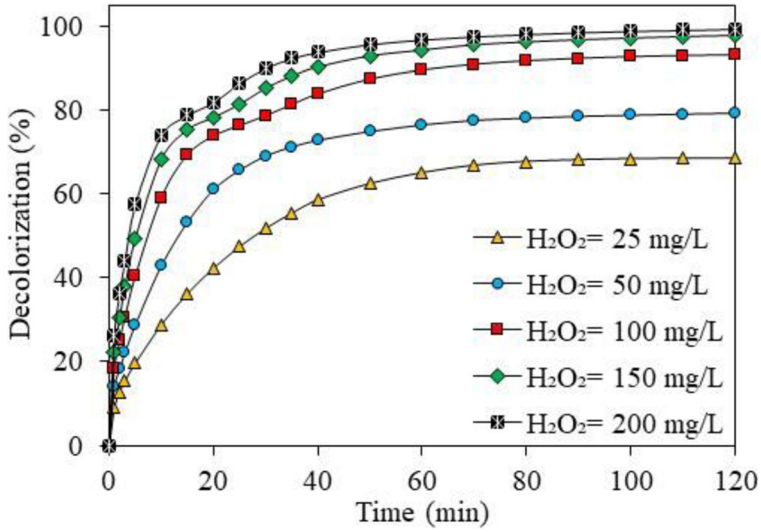

Fig. 8 Effect of H_2O_2 on the decolorization (RB19 = 100 mg/L, Fe(II) = 10 mg/L, pH = 3, Temperature = 20 °C)

120 min with 100, 150, 200, and 300 mg/L RB19, respectively. With these results, it is clearly understood that increasing initial RB19 concentration reduces the decolorization. The reason for this is that the other parameters (Fe(II) and H_2O_2) were kept fixed while the pollutant concentration increased (Li et al. 2015). In other words, as the concentration of hydroxyl radicals produced by the fixed H_2O_2 and Fe(II) concentrations was the same, decolorization reduced with the increase in RB19 concentration.

3.6 Effect of Temperature

An important parameter for removal of pollutants with the Fenton oxidation process is temperature. With this aim, a range of experiments were performed at different temperatures (10, 20, 30, and 40 °C) and the results are shown in Fig. 10. The increase in temperature was clearly observed to increase the decolorization rate. The reason for this is that the temperature increase increased the reaction rate between H_2O_2 and Fe(II), and this forms higher amounts of hydroxyl radicals (Bagal and Gogate 2014; Mirzaei et al. 2017). Additionally, the system may be operated at higher temperatures to ensure the decolorization in shorter durations. The increase in temperature from 10 to 40 °C was not observed to have a significant effect on the decolorization at the end of 120 min. However, at the end of 20 min, the decolorization was 31.2% at 10 °C, while decolorization was 82.9% at 40 °C. Based on these results, at the end of

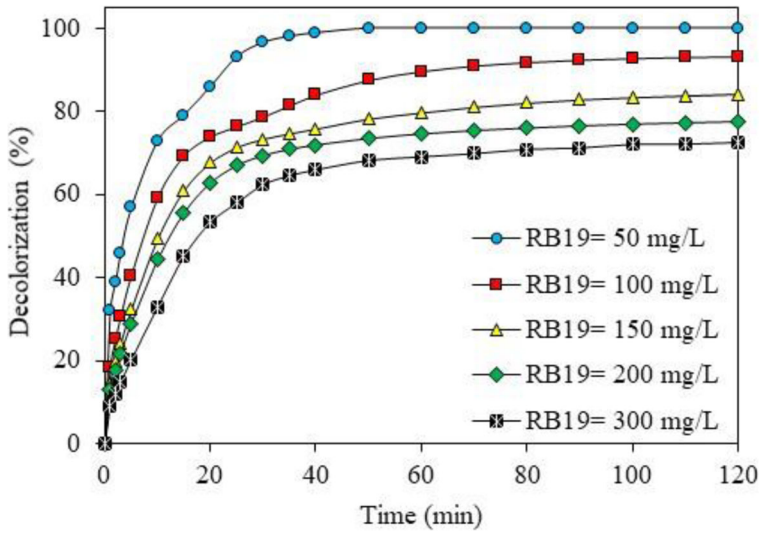

Fig. 9 Effect of initial RB19 concentration on the decolorization (H_2O_2 = 100 mg/L, Fe(II) = 10 mg/L, pH = 3, Temperature = 20 °C)

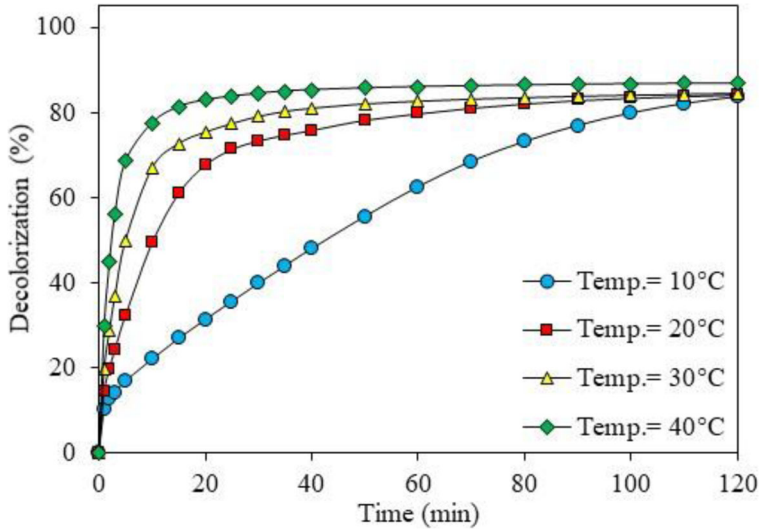

Fig. 10 Effect of temperature on the decolorization (RB19 = 150 mg/L, H_2O_2 = 100 mg/L, Fe(II) = 10 mg/L, pH = 3)

reaction durations of 60 min or longer, temperature increases above 20 °C can be said not to significantly affect the system performance. Additionally, due to rapid separation of H_2O_2 into water and oxygen at much higher temperatures, the effective use of H_2O_2 reduces (Babuponnusami and Muthukumar 2014).

4 Conclusion

Based on the experimental results, decolorization of RB19 from aqueous solutions was successfully completed with the Fenton oxidation process. Initial pH, H_2O_2 concentration, Fe(II) concentration, DOHF concentration, and temperature were found to have strong effects on the decolorization. With H_2O_2 concentration 100 mg/L, Fe(II) concentration 10 mg/L, pH 3, temperature 20 °C, and 60 min reaction duration, 100% decolorization was obtained for 50 mg/L RB19 concentration. The decolorization of RB19 reduced with the increase in initial RB19 concentration and increased with the increases in reaction temperature and H_2O_2 concentration. Additionally, the DNN-based modeling providing the best performance was researched for this subject. According to the experimental results, the DNN model having the seven hidden layers, relu activation function and RMSProp optimization function provided the best performance in terms of minimum RMSE and maximum R^2. The model's success is acceptable, but it should be noted that the limited number of input variables and data noise could also negatively affect the results. Recalibration of the model would be required in future studies for a more accurate prediction model. Additionally, other input parameters may also be considered for future modeling works. So, future studies could be more effective for decolorization with the Fenton process than the current results.

References

Alalm, M. G., Tawfik, A., & Ookawara, S. (2015). Degradation of four pharmaceuticals by solar photo-Fenton process: kinetics and costs estimation. *Journal of Environmental Chemical Engineering, 3*(1), 46–51.

Alexander, D. L. J., Tropsha, A., & Winkler, D. A. (2015). Beware of R^2: Simple, unambiguous assessment of the prediction accuracy of QSAR and QSPR models. *Journal of Chemical Information and Modeling, 55*(7), 1316–1322.

Alver, A., & Kazan, Z. (2020). Prediction of full-scale filtration plant performance using artificial neural networks based on principal component analysis. *Separation and Purification Technology*. https://doi.org/10.1016/j.seppur.2019.115868.

Azbar, N., Yonar, T., & Kestioglu, K. (2004). Comparison of various advanced oxidation processes and chemical treatment methods for COD and color removal from a polyester and acetate fiber dyeing effluent. *Chemosphere, 55*(1), 35–43.

Babuponnusami, A., & Muthukumar, K. (2014). A review on Fenton and improvements to the Fenton process for wastewater treatment. *Journal of Environmental Chemical Engineering, 2*(1), 557–572.

Bae, W., Won, H., Hwang, B., de Toledo, R. A., Chung, J., Kwon, K., et al. (2015). Characterization of refractory matters in

dyeing wastewater during a full-scale Fenton process following pure-oxygen activated sludge treatment. *Journal of Hazardous Materials, 287*, 421–428.

Bagal, M. V., & Gogate, P. R. (2014). Wastewater treatment using hybrid treatment schemes based on cavitation and Fenton chemistry: a review. *Ultrasonics Sonochemistry, 21*(1), 1–14.

Baştürk, E., & Alver, A. (2019). Modeling azo dye removal by sono-Fenton processes using response surface methodology and artificial neural network approaches. *Journal of Environmental Management*. https://doi.org/10.1016/j.jenvman.2019.109300.

Bautista, P., Mohedano, A. F., Gilarranz, M. A., Casas, J. A., & Rodriguez, J. J. (2007). Application of Fenton oxidation to cosmetic wastewaters treatment. *Journal of Hazardous Materials, 143*(1–2), 128–134.

Bayhan, Y. K., & Degermenci, G. D. (2017). Investigation of kinetic and removal of organic matter from cosmetic wastewaters by Fenton process. *Journal of the Faculty of Engineering and Architecture of Gazi University*. https://doi.org/10.17341/gazimmfd.300609.

Behnajady, M. A., Modirshahla, N., & Ghanbary, F. (2007). A kinetic model for the decolorization of CI acid yellow 23 by Fenton process. *Journal of Hazardous Materials, 148*(1–2), 98–102.

Bhatti, A. A., Kamboh, M. A., Solangi, I. B., & Memon, S. (2013). Synthesis of calix [6] arene based XAD-4 material for the removal of reactive blue 19 from aqueous environments. *Journal of Applied Polymer Science, 130*(2), 776–785.

Chang, M. W., & Chern, J. M. (2010). Decolorization of peach red azo dye, HF6 by Fenton reaction: Initial rate analysis. *Journal of the Taiwan Institute of Chemical Engineers, 41*(2), 221–228.

Chavaco, L. C., Arcos, C. A., & Prato-Garcia, D. (2017). Decolorization of reactive dyes in solar pond reactors: perspectives and challenges for the textile industry. *Journal of Environmental Management*. https://doi.org/10.1016/j.jenvman.2017.04.077.

Daneshvar, N., Khataee, A. R., & Djafarzadeh, N. (2006). The use of artificial neural networks (ANN) for modeling of decolorization of textile dye solution containing CI basic yellow 28 by electrocoagulation process. *Journal of Hazardous Materials, 137*(3), 1788–1795.

Değermenci, G. D., Değermenci, N., Ayvaoğlu, V., Durmaz, E., Çakır, D., & Akan, E. (2019). Adsorption of reactive dyes on lignocellulosic waste; characterization, equilibrium, kinetic and thermodynamic studies. *Journal of Cleaner Production, 225*, 1220–1229.

Elmolla, E. S., Chaudhuri, M., & Eltoukhy, M. M. (2010). The use of artificial neural network (ANN) for modeling of COD removal from antibiotic aqueous solution by the Fenton process. *Journal of Hazardous Materials, 179*(1–3), 127–134.

Emami, F., Tehrani-Bagha, A. R., Gharanjig, K., & Menger, F. M. (2010). Kinetic study of the factors controlling Fenton-promoted destruction of a non-biodegradable dye. *Desalination, 257*(1–3), 124–128.

Fanchiang, J. M., & Tseng, D. H. (2009). Degradation of anthraquinone dye CI reactive blue 19 in aqueous solution by ozonation. *Chemosphere, 77*(2), 214–221.

Ghosh, P., Samanta, A. N., & Ray, S. (2010). COD reduction of petrochemical industry wastewater using Fenton's oxidation. *The Canadian Journal of Chemical Engineering, 88*(6), 1021–1026.

Hayat, H., Mahmood, Q., Pervez, A., Bhatti, Z. A., & Baig, S. A. (2015). Comparative decolorization of dyes in textile wastewater using biological and chemical treatment. *Separation and Purification Technology, 154*, 149–153.

Hu, Q. H., Qiao, S. Z., Haghseresht, F., Wilson, M. A., & Lu, G. Q. (2006). Adsorption study for removal of basic red dye using bentonite. *Industrial & Engineering Chemistry Research, 45*(2), 733–738.

Kavitha, V., & Palanivelu, K. (2005). Destruction of cresols by Fenton oxidation process. *Water Research, 39*(13), 3062–3072.

Khan, J., Sayed, M., Ali, F., & Khan, H. M. (2018). Removal of acid yellow 17 dye by Fenton oxidation process. *Zeitschrift für Physikalische Chemie, 232*(4), 507–525.

Li, H., Li, Y., Xiang, L., Huang, Q., Qiu, J., Zhang, H., et al. (2015). Heterogeneous photo-Fenton decolorization of Orange II over Al-pillared Fe-smectite: response surface approach, degradation pathway, and toxicity evaluation. *Journal of Hazardous Materials, 287*, 32–41.

Lin, S. H., & Leu, H. G. (1999). Operating characteristics and kinetic studies of surfactant wastewater treatment by Fenton oxidation. *Water Research, 33*(7), 1735–1741.

Lin, S. H., & Lo, C. C. (1997). Fenton process for treatment of desizing wastewater. *Water Research, 31*(8), 2050–2056.

Lucas, M. S., & Peres, J. A. (2006). Decolorization of the azo dye reactive black 5 by Fenton and photo-Fenton oxidation. *Dyes and Pigments, 71*(3), 236–244.

Michael, I., Hapeshi, E., Michael, C., & Fatta-Kassinos, D. (2010). Solar Fenton and solar TiO_2 catalytic treatment of ofloxacin in secondary treated effluents: evaluation of operational and kinetic parameters. *Water Research, 44*(18), 5450–5462.

Mirzaei, A., Chen, Z., Haghighat, F., & Yerushalmi, L. (2017). Removal of pharmaceuticals from water by homo/heterogonous Fenton-type processes–a review. *Chemosphere, 174*, 665–688.

Mousavi, S. A., Vasseghian, Y., & Bahadori, A. (2018). Evaluate the performance of Fenton process for the removal of methylene blue from aqueous solution: experimental, neural network modeling and optimization. *Environmental Progress & Sustainable Energy*. https://doi.org/10.1002/ep.13126.

Nidheesh, P. V., Zhou, M., & Oturan, M. A. (2018). An overview on the removal of synthetic dyes from water by electrochemical advanced oxidation processes. *Chemosphere, 197*, 210–227.

Özdemir, C., Tezcan, H., Sahinkaya, S., & Kalipci, E. (2010). Pretreatment of olive oil mill wastewater by two different applications of Fenton oxidation processes. *CLEAN–Soil Air Water, 38*(12), 1152–1158.

Radwan, M., Alalm, M. G., & Eletriby, H. (2018). Optimization and modeling of electro-Fenton process for treatment of phenolic wastewater using nickel and sacrificial stainless steel anodes. *Journal of Water Process Engineering, 22*, 155–162.

Ravì, D., Wong, C., Deligianni, F., Berthelot, M., Andreu-Perez, J., Lo, B., et al. (2016). Deep learning for health informatics. *IEEE Journal of Biomedical and Health Informatics, 21*(1), 4–21.

Şahinkaya, S. (2013). COD and color removal from synthetic textile wastewater by ultrasound assisted electro-Fenton

oxidation process. *Journal of Industrial and Engineering Chemistry, 19*(2), 601–605.

Sanchis, S., Polo, A. M., Tobajas, M., Rodriguez, J. J., & Mohedano, A. F. (2014). Coupling Fenton and biological oxidation for the removal of nitrochlorinated herbicides from water. *Water Research, 49*, 197–206.

Shi, X., Tian, A., You, J., Yang, H., Wang, Y., & Xue, X. (2018). Degradation of organic dyes by a new heterogeneous Fenton reagent-Fe_2GeS_4 nanoparticle. *Journal of Hazardous Materials, 353*, 182–189.

Siddique, M., Farooq, R., & Price, G. J. (2014). Synergistic effects of combining ultrasound with the Fenton process in the degradation of reactive blue 19. *Ultrasonics Sonochemistry, 21*(3), 1206–1212.

Slokar, Y. M., & Le Marechal, A. M. (1998). Methods of decoloration of textile wastewaters. *Dyes and Pigments, 37*(4), 335–356.

Sun, J. H., Sun, S. P., Wang, G. L., & Qiao, L. P. (2007). Degradation of azo dye Amido black 10B in aqueous solution by Fenton oxidation process. *Dyes and Pigments, 74*(3), 647–652.

Sun, S. P., Li, C. J., Sun, J. H., Shi, S. H., Fan, M. H., & Zhou, Q. (2009). Decolorization of an azo dye Orange G in aqueous solution by Fenton oxidation process: effect of system parameters and kinetic study. *Journal of Hazardous Materials, 161*(2–3), 1052–1057.

Suteu, D., Bilba, D., Aflori, M., Doroftei, F., Lisa, G., Badeanu, M., et al. (2012). The seashell wastes as biosorbent for reactive dye removal from textile effluents. *CLEAN–Soil Air Water, 40*(2), 198–205.

Titouhi, H., & Belgaied, J. E. (2016). Heterogeneous Fenton oxidation of ofloxacin drug by iron alginate support. *Environmental Technology, 37*(16), 2003–2015.

Vilar, A., Eiroa, M., Kennes, C., & Veiga, M. C. (2013). Optimization of the landfill leachate treatment by the Fenton process. *Water and Environment Journal, 27*(1), 120–126.

Wang, J., Jiang, Y., Zhang, Z., Zhang, X., Ma, T., Zhang, G., et al. (2007). Investigation on the sonocatalytic degradation of acid red B in the presence of nanometer TiO_2 catalysts and comparison of catalytic activities of anatase and rutile TiO_2 powders. *Ultrasonics Sonochemistry, 14*(5), 545–551.

Willmott, C. J., & Matsuura, K. (2005). Advantages of the mean absolute error (MAE) over the root mean square error (RMSE) in assessing average model performance. *Climate Research, 30*(1), 79–82.

Xie, X., Zheng, X., Yu, C., Zhang, Q., Wang, Y., Cong, J., et al. (2019). Tea residue boosts dye decolorization and induces the evolution of bacterial community. *Water Air & Soil Pollution*. https://doi.org/10.1007/s11270-019-4307-6.

Zhang, H., Duan, L., & Zhang, D. (2006). Decolorization of methyl orange by ozonation in combination with ultrasonic irradiation. *Journal of Hazardous Materials, 138*(1), 53–59.